CDF/PHYS/BOTTOM/CDFR/4696
Version 1.0
August 10, 1998

Simulation of a Time-of-Flight Detector for Physics Studies at CDF

M. Jones, J. Kroll, C. Chen
University of Pennsylvania

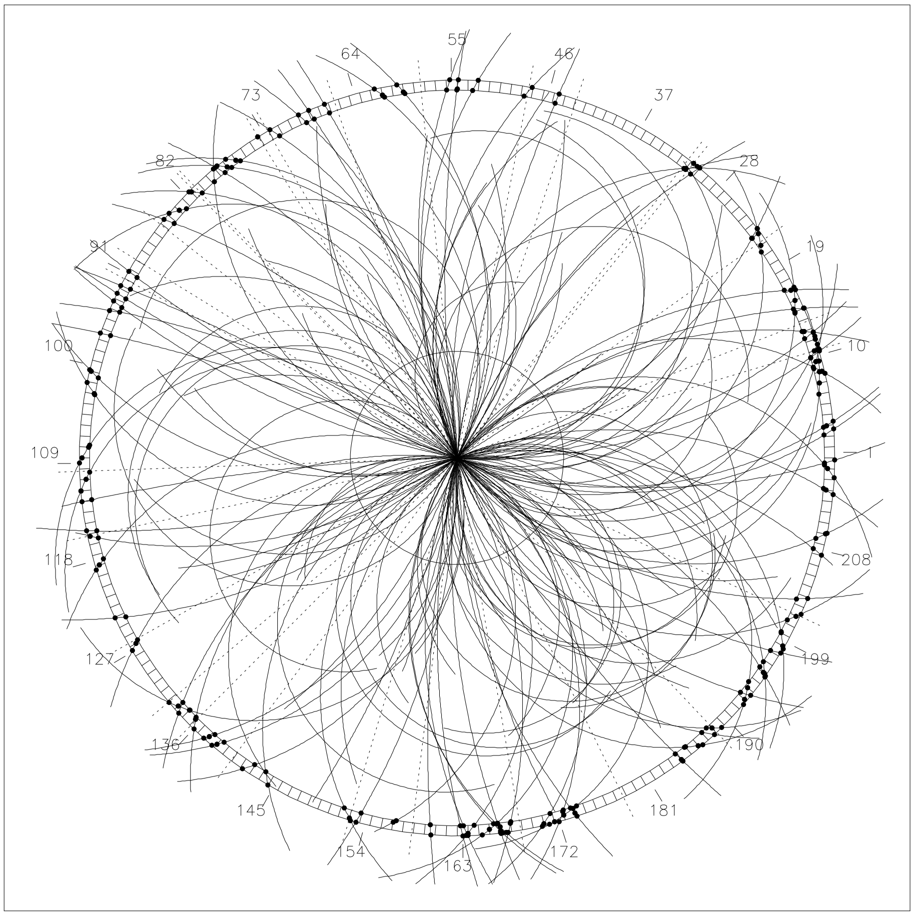

1 Introduction

One of the primary goals of the Run II B-physics program is to study CP violation and mixing in the B-system. Particle identification has the potential to greatly enhance this effort in a number of ways. The ability to distinguish kaons from pions will be a powerful tool for for the reconstruction of many exclusive final states. However, the primary goal of our recent physics studies was to quantify the impact that particle identification would have on our ability to tag the production flavor of B_d and B_s mesons.

The most economical way to provide CDF with the capability of particle identification is with a Time-of-Flight (TOF) detector. This would consist of bars of scintillator with photomultiplier tubes (PMT's) at each end and would be located in the space between the COT can and the cryostat. This system was originally proposed in[1] and a test system, consisting of 20 bars of scintillator, was installed at the end of Run Ib[2]. At this time, a TOF system is being considered as an upgrade for Run II which lies beyond CDF's baseline detector configuration.

To understand how this project would enrich CDF's B-physics program we have written a Monte Carlo which simulates many of the relevant features of the proposed TOF systems under consideration. In this note we provide details of this simulation and use it to study algorithms for performing event reconstruction and kaon identification. Based on these algorithms, particle identification is applied to various techniques for B-flavor tagging, the results of which are presented in a separate note[3]. Although motivated by flavor tagging studies, this Monte Carlo is suitable for the study of a wide range of physics topics.

2 Proposed TOF systems

The TOF system originally proposed[1] would consist of 216 bars of scintillator with a trapezoidal cross section of approximately 4 cm $\times$ 4 cm and a length of 300 cm. These would have mesh PMT's attached to each end and would be placed parallel to the beam axis between the COT and the inner wall of the cryostat as shown schematically in figure 1.

In the event that 3 m bars cannot be installed at the start of Run II, an alternative plan has been considered. This is motivated by the fact that once the end plug calorimeters are in place, their limit of travel is only 62 inches. Hence, once in place, they cannot be rolled out far enough to allow 3 m bars to be inserted. This problem can be circumvented if a TOF system consisting of short bars, 130 cm in length is considered, which can be inserted as shown in figure 2.

However, in this scenario, the length of the COT would be covered by two short bars and with PMT's at the end of each bar, the number of PMT's and electronics channels required would be doubled. Nevertheless, as there are potential advantages to the higher segmentation of such a system, we simulate both long and short bar geometries in the Monte Carlo. Several of the physics studies performed were concerned with understanding the differences in performance one might expect from these two configurations.

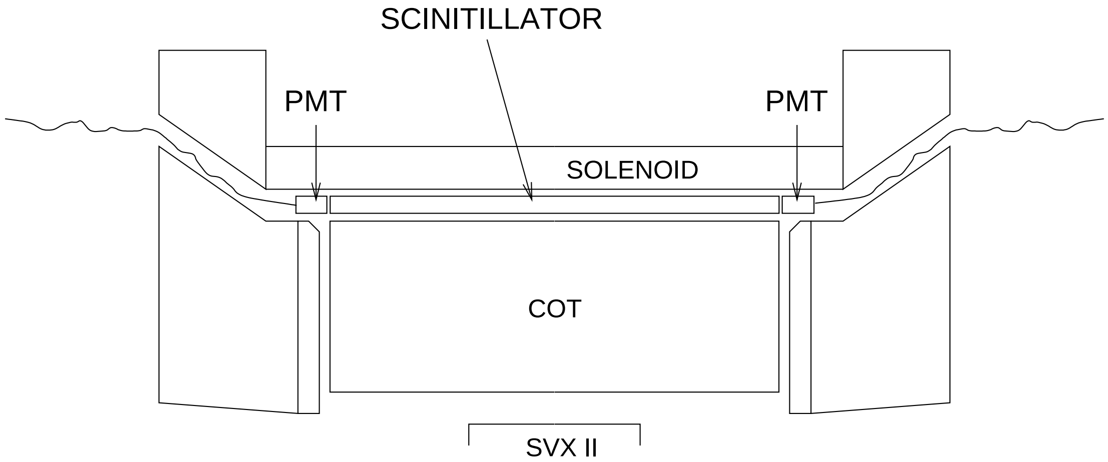

Figure 1: A schematic view of the CDF detector showing the location of the scintillator bars and PMT's for a 3 m bar TOF system.

3 TOF simulation

This section describes the features included in the Monte Carlo. The simulation was intended to be simple, but at the same time to include as many of the effects relevant for understanding the performance of the proposed TOF systems as were appropriate. Although future studies will likely require full tracking simulations and a GEANT based detector model, this simple simulation will be very useful for understanding results obtained from a more complicated Monte Carlo.

The simulation is performed within the framework of Analysis Control and calculates the times at which the PMT's at the ends of the bars would fire their discriminators, based on information in the `/HEPEVT/` common block. As we do not intend to use multi-hit electronics, only the first hit on a PMT can be used for TOF measurements.

3.1 TOF system geometries

Both the long (3 m) and the short (130 cm) TOF system geometries are simulated. The short bar geometry has an uninstrumented region between $z = -20$ and $z = 20$ cm, occupied by the PMT and preamp assemblies, while the long bar geometry covers the full length of the COT. Both geometries have the inner and outer surfaces of the bars located at radii of 138.0 and 141.8 cm and have this annular region subdivided into 216 bars in φ. The wrapping material on the bars is expected to be about 140 μm thick and would occupy only 0.7% of the available azimuthal space. This material has been ignored and we do not simulate any cracks between the bars in φ.

3.2 Generation of hits

The helical trajectories of charged particles in the `/HEPEVT/` common block are used to determine the points at which they enter and exit the scintillator bars. The momentum, particle type, path length and production time are used to calculate the time at which

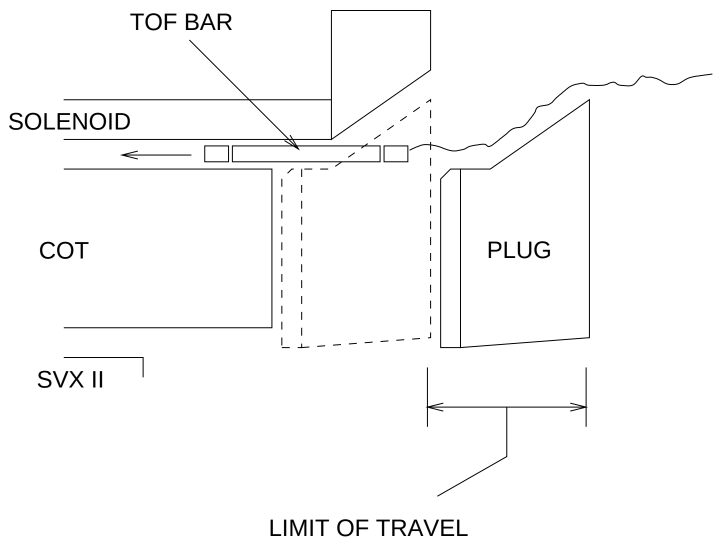

Figure 2: The proposed installation scenario for a TOF system consisting of short (130 cm) scintillator bars.

a track enters a bar. The energy deposited in the bar is then calculated from the path length of the track in the bar and dE/dx, calculated using the Bethe-Bloch equation, which gives about 2 MeV/cm for a MIP in polyvinyltoluene. The light generated at the entrance position of a track is propagated to the ends of the bar with a constant speed 14 cm/ns and is attenuated using the attenuation length for BC408 of 300 cm. The time recorded by a PMT is the first time at which light above a nominal threshold of 0.4 MeV (5% MIP at normal incidence) reaches the end of the bar.

3.3 Timing resolution

The timing resolution is parameterized by

$$\sigma_T = \left(\sigma_0 + \frac{d\sigma}{dz}d\right)\sqrt{\frac{8\text{ MeV}}{Q}} \tag{1}$$

where $\sigma_0 + d\sigma/dz \cdot d$ is a linear dependence of resolution with distance and the square root term accounts for the dependence on photon statistics according to the energy, Q, deposited in the bar. The values of these parameters were $\sigma_0 = 100$ ps and $d\sigma/dz = 0.4$ ps/cm, with which most physics studies were performed. This is a conservative parameterization of the expected timing resolution.

3.4 Photon conversion

Photon conversion is considered in either the outer skin of the COT (1/4 in of aluminum, 0.071 X_0) or in the scintillator itself (4 cm polyvinyltoluene, 0.094 X_0). Photons which convert are replaced by an electron-positron pair at the conversion point which share the photon energy equally. These generate light in the scintillator and hits in the PMT's as would other charged tracks. A more realistic treatment would track the electron-positron

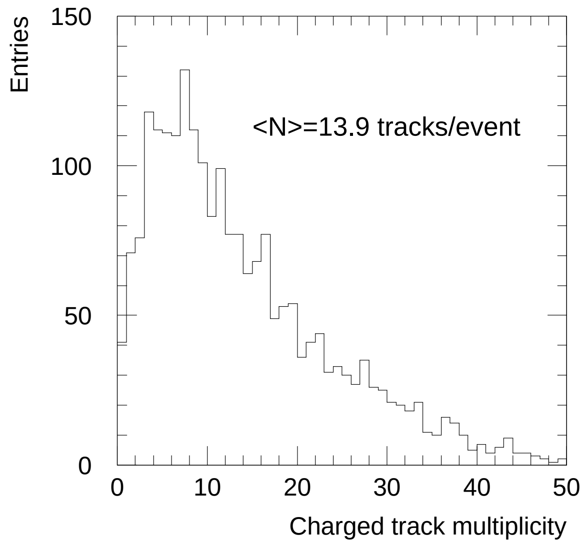

Figure 3: Charged track multiplicity distribution for selected minimum bias events.

pairs produced by conversions in all material upstream of the scintillator but this would be more easily treated in the context of a GEANT based simulation.

3.5 Minimum bias events

Tracks from minimum bias data are mixed with the generated `/HEPEVT/` event record. The minimum bias events were selected from runs 58817 and 59093 and were required to have exactly one primary vertex within 60 cm of the origin in z. The charged track multiplicity distribution for these events is shown in figure 3 and has a mean of 14. For each selected event, all tracks had their track parameters written to a file, with their transverse and longitudinal impact parameters set to zero.

At low p_T, there is an asymmetry in the number of positive and negative tracks reconstructed in these events which could potentially bias our estimates of B-flavor tagging dilution. We have removed this asymmetry by randomly reversing the charge of a fraction of positive tracks to give, on average, equal numbers of positive and negative tracks for all p_T.

In the studies described here, the number of additional minimum bias events added to the `/HEPEVT/` event record is determined from a Poisson distribution with mean $\langle n_{\rm mb}\rangle$. The values of $\langle n_{\rm mb}\rangle$ are chosen to be 2, 5 or 10 which correspond to the luminosity scenarios shown in Table 1. Masses were assigned to the tracks such that the resulting sample was 83% pions, 10% kaons and 7% protons [4].

$\mathcal{L}$ (cm^{-2}s^{-1})	$\tau_{\rm bc}$ (ns)	$\langle n_{\rm mb}\rangle$
$.5\times 10^{32}$	396	2
2×10^{32}	396	5
2×10^{32}	132	2
10×10^{32}	132	10

Table 1: Expected $\langle n_{\rm mb}\rangle$ for different luminosities and times between bunch crossings.

The proton bunch lengths are expected to remain constant at $\sim$ 40 cm throughout a fill, while the antiproton bunch length may vary from $\sim$ 70 cm at the start of a fill to $\sim$ 50 cm at the end. When mixing minimum bias events, the width of the antiproton bunch is chosen uniformly between these limits. The minimum bias events are then placed at random positions in z and t generated from the distribution

$$f_{p\overline{p}}(u,v) = \frac{1}{2\pi\sigma_p\sigma_{\overline{p}}} e^{-u^2/2\sigma_p^2} e^{-v^2/2\sigma_{\overline{p}}^2} \qquad (2)$$

where $u = z - ct$ and $v = z + ct$.

3.6 Kaon and pion decay

A non-negligible fraction of low momentum kaons can decay before reaching the scintillator. Not all the information from these tracks will be lost, however, and we account for this in the following way. If a K^+ decays into either $\mu^+\nu_\mu$ or $\pi^+\pi^0$ before reaching the scintillator the component of the μ^+ or π^+ momentum along the original flight direction is calculated. If this is negative, the track is considered to be lost and it will not generate hits in TOF. If it is positive, the time at which it hits the scintillator is determined by supposing that it followed the helical trajectory which would have been followed by the kaon. For the other the other 15% of its decay modes, the kaon is also considered to be lost and will not generate TOF hits.

While this is clearly an oversimplification of the situation we have not intended to provide a full tracking simulation. This level of sophistication would be best handled within the framework of a GEANT based physics study which would include a more complete tracking and event reconstruction simulation.

So as not to underestimate the track mulitplicity due to minimum bias events, tracks added to the `/HEPEVT/` event record from minimum bias data are not allowed to decay, even if they were assigned the kaon mass.

3.7 Impact parameter resolution

Although a full tracking simulation is not performed, the impact parameters D_0 and Z_0 are smeared by their expected resolutions which depend on whether a track passes through an SVX-II hybrid chip. Hybrid chips are 5 cm long and are located at the ends of the three silicon ladders which are ~ 30 cm in length at a mean radius of 2.8 cm. When a track does not hit a hybrid chip, the resolution is parametrized by

$$\sigma_{D_0} = 13 + 40/p_T \ \mu\mathrm{m} \quad (3)$$
$$\sigma_{Z_0} = 28 + 40/p_T \ \mu\mathrm{m}, \quad (4)$$

where p_T is in GeV/c, and by

$$\sigma_{D_0} = 13 + 80/p_T \ \mu\mathrm{m} \quad (5)$$
$$\sigma_{Z_0} = 28 + 80/p_T \ \mu\mathrm{m} \quad (6)$$

when a hybrid chip is hit. Our analyses of flavor tagging consider the additional benefit which would be gained by silicon layer 00. There are currently two possible scenarios for layer 00, one which places the additional silicon layer at a radius of 1.7 cm and the other at a radius of 1.4 cm. The impact parameter resolution for either of these scenarios is expected to be roughly as follows:

$$\sigma_{D_0} = 5.5 + 17/p_T \ \mu\mathrm{m}. \quad (7)$$

In all cases, it is assumed that the position of the primary vertex can be measured with resolutions of 10 μm in r-φ and 30 μm in the r-z plane, as was done in previous studies of proper time resolution for B_s^0 decays [5]. In the description of our flavor tagging studies[3], we use the impact parameters to distinguish tracks from B-decays from fragmentation tracks. Thus, these resolutions are added in quadrature to σ_{D_0} and σ_{Z_0} to obtain the expected resolutions of impact parameters with respect to the position of the primary vertex.

4 Event reconstruction

We do not assume perfect association between tracks and the PMT's which register the light they generate. Instead, we consider two algorithms for making this association, upon which the reconstruction of real events would likely be based.

The first associates both PMT's at the ends of a bar with a track if the z-position at which the track entered the bar matches the z-position determined by $T_L - T_R$ to within 2σ. We refer to this method as the "$T_L - T_R$" algorithm. In general, only bars which are hit by single tracks will be used and the efficiency with which a track can be associated to a bar is reduced for high luminosities.

Figure 4a shows the efficiency for associating hits with charged tracks which hit at least one bar. Because of the gap between $z = -20$ cm and $z = 20$ cm for a short bar system, the efficiency for associating hits with tracks is 15% lower than for a system with 3 m bars. The track-hit association efficiency for short bars relative to a long bar system is shown by the solid circles in figure 4a. Figure 4b shows the fraction of tracks which had at least one misassigned hit.

We have also considered alternative algorithms for associating hits with tracks which attempt to make use of bars in which light from a track is registered by only one PMT. One method associates a PMT to the closest track in z, if there are no other tracks which hit the bar within 30 cm in z. We refer to this as the "closest track" algorithm. The procedure

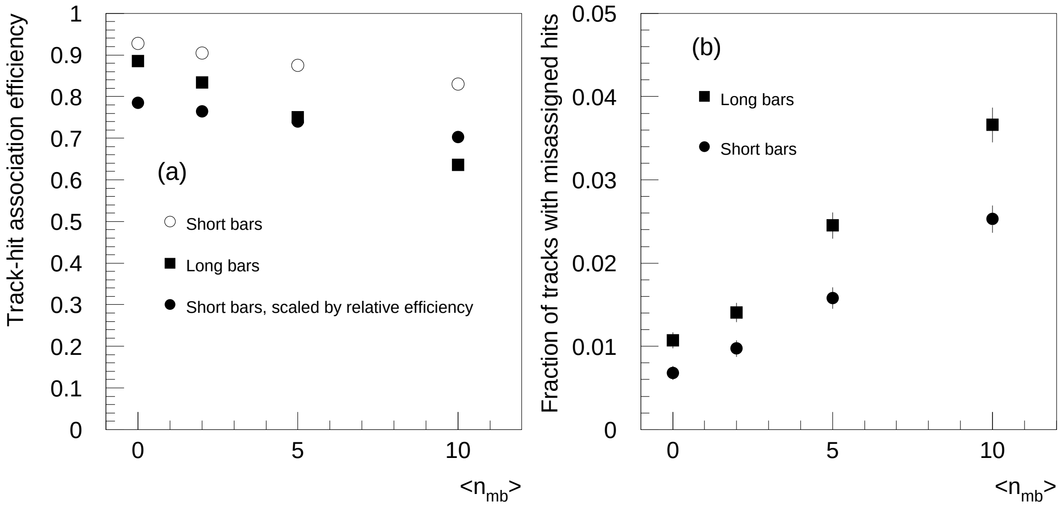

Figure 4: Track hit association efficiency and misassociation fraction for long and short bar TOF systems as functions of the mean number of minimum bias events, $\langle n_{\rm mb} \rangle$. Track-hit association is performed based on the "$T_L - T_R$" matching algorithm.

usually gives the correct association since the range of event t_0's ($<$ 3 ns) and flight times ($<$ 10 ns) will be somewhat shorter than the time taken by light to propagate to the ends of the bars ($<$ 20 ns for long bars). When only one track hits a bar this algorithm always associates both PMT's to the track but when there are multiple tracks in a bar, the ones closest to the ends will only be associated with a single PMT and consequently their timing resolution will be degraded. The efficiency with which this algorithm associates hits with tracks and the fraction of associations with misassigned hits is shown in figure 5. The "closest track" algorithm is seen to provide both higher efficiency and a lower misassociation rate than the "$T_L - T_R$" method.

From these figures we conclude that the loss of tracks with TOF hits should not be a major concern even at very high luminosities. However, although 90% of tracks may have at least one PMT associated with them in a long bar system, even when $\mathcal{L} = 10^{33}$ cm^{-2}s^{-1}, the average timing resolution will be degraded since fewer tracks will be associated with both PMT's. The impact that this will have on the purity of a kaon sample is examined in section 6.

It is also useful to consider the average occupancy expected for the long and short bar TOF systems for the various luminosity scenarios. Here we define the average occupancy as the number of TOF bars hit by more than one track divided by the number hit by exactly one track. Figure 6 shows this measure of the average occupancy as a function of the number of minimum bias events for long and short TOF bars. Comparing figure 6 with figure 5 shows that even when the average occupancy is rather high, we can still associate a large fraction of the tracks with at least one PMT for both long and short bar systems.

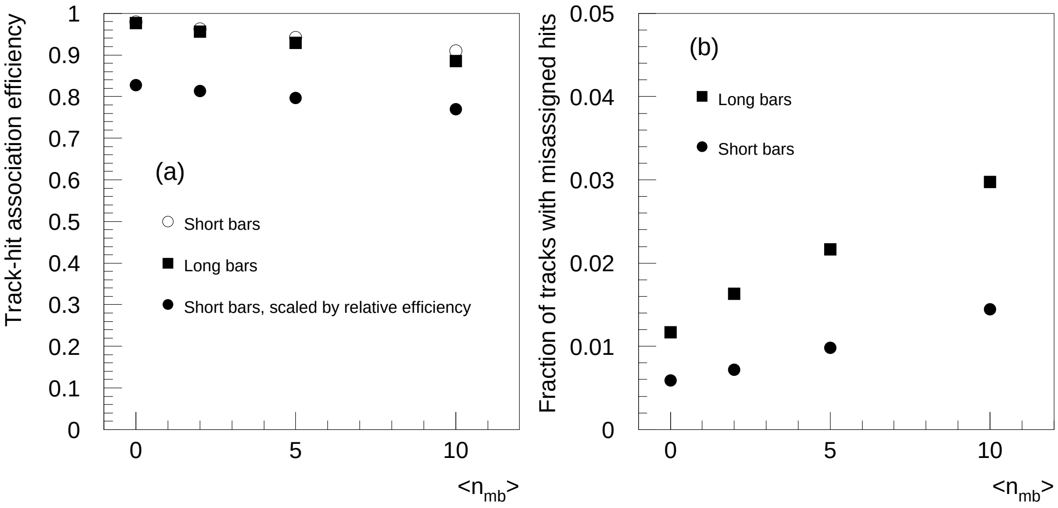

Figure 5: Track hit association efficiency and misassociation fraction for long and short bar TOF systems as functions of the mean number of minimum bias events, $\langle n_{\mathrm{mb}} \rangle$. Track-hit association is performed based on the "closest track" matching algorithm.

5 Determination of t_0

For high luminosity running we expect the mean number of $p\overline{p}$ interactions per event to be between 2 and 5. In general, we may need to determine the z-coordinate and t_0 of each interaction in the event. However, for analyses in which a B decay is fully reconstructed it will be sufficient to identify tracks associated with its primary interaction vertex. So far we have only considered the latter case.

The average production time for the tracks in a $B^0 \to J/\psi K^0_{\mathrm{S}}$ decay already determines the t_0 of the event with a resolution of about 63 ps. This is sufficient to identify tracks in the event which have production times consistent with the t_0 of the $J/\psi K^0_{\mathrm{S}}$ primary vertex. These tracks are used in the t_0 fit if their transverse and longitudinal impact parameters are within 0.5 cm and 1.0 cm of the J/ψ vertex, respectively, and if their production time, under any of the π, K or p hypotheses, is within 5σ of the $J/\psi K^0_{\mathrm{S}}$ t_0 estimate.

Figure 7 shows the t_0 distributions for both the $J/\psi K^0_{\mathrm{S}}$ alone and for the full event, obtained by fitting t_0 using tracks associated with the $J/\psi K^0_{\mathrm{S}}$ production vertex. The t_0 resolution is found to be about 33 ps which is similar to previous expectations [1]. This figure also shows the distribution of the number of tracks used in the fit. This has a mean of 10, in addition to the J/ψ and K^0_{S} tracks.

The fit is performed by first computing the expected production times for each track under assumed particle hypotheses:

$$t_i^h = T_i - D/c\sqrt{1 + m_h^2/p^2} \tag{8}$$

where T_i is the time recorded by the TOF counters, D is the path length of the track from the production point to the counter and p is its momentum.

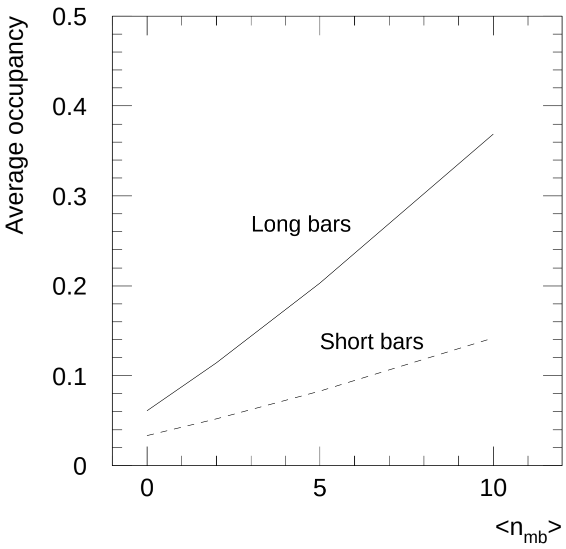

Figure 6: Average occupancy for long and short bar TOF systems as a function of the number of minimum bias events.

Then, the t_0 for the interaction is determined by maximizing the likelihood function

$$\mathcal{L} = \frac{1}{\sqrt{2\pi}\sigma_t} e^{-(t_{J/\psi K_S^0} - t_0)^2/2\sigma_t^2} \cdot \prod_i \left(f_\pi \mathcal{L}_\pi(t_i^\pi, \sigma_{t_i}; t_0) + f_K \mathcal{L}_K(t_i^K, \sigma_{t_i}; t_0) + f_p \mathcal{L}_p(t_i^p, \sigma_{t_i}; t_0) \right) \quad (9)$$

where $t_{J/\psi K_S^0}$ is the measured production time of the $J/\psi K_{\mathrm{S}}^0$ with uncertainty σ_t, f_h are assumed particle production fractions and

$$\mathcal{L}_h(t^h, \sigma_t; t_0) = \frac{1}{\sqrt{2\pi}\sigma_t} e^{-(t^h - t_0)^2/2\sigma_t^2}. \quad (10)$$

The particle fractions were fixed at $f_\pi = 0.7$, $f_K = 0.2$ and $f_p = 0.1$ but the fit is not particularly sensitive to the exact values used.

6 Particle identification strategies

The information provided by time of flight can be used in a variety of ways to select pure samples of kaons. One procedure is to define a probability weight w_i, by constructing the χ^2 from the significance of the difference between the event t_0 and a track's production time, calculated using its momentum, path length, time of flight and an assumed mass hypothesis, i. The weight is the area in the tail of a χ^2 distribution above this value. Probability weights are distributed uniformly between 0 and 1 for correct mass assignments. The efficiency for selecting kaons by applying the cut $w_K > w_K^{\mathrm{cut}}$ is then $1 - w_K^{\mathrm{cut}}$.

The χ^2 values can also be used to define likelihoods L_i for each hypothesis i,

$$L_i = \exp(-\chi_i^2/2) \quad (11)$$

which can then used to define the normalized likelihood λ_i,

$$\lambda_i = \frac{f_i L_i}{\sum_j f_j L_j} \quad (12)$$

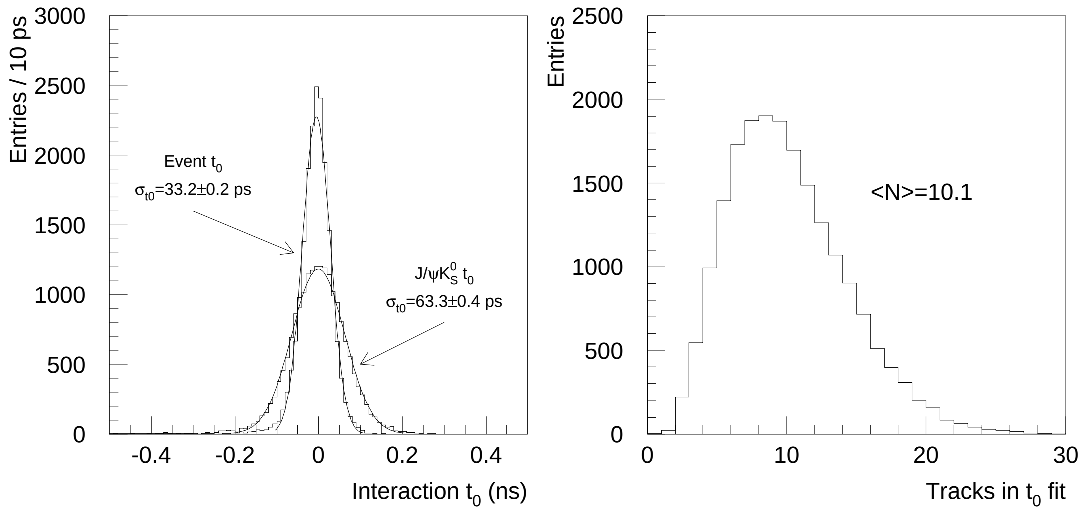

Figure 7: Fitted t_0 distributions for $J/\psi K^0_S$ and for the full event. Also shown is the distribution of the number of tracks used in the event t_0 fit in addition to the tracks from the $B^0 \to J/\psi K^0_S$ decay.

where f_j are production fractions of the various particle species which can depend on the class of tracks being considered. In practice, they would be measured for a particular class of tracks but here we parameterize p_T dependent fractions from our Monte Carlo sample to define the normalized likelihood. These fractions and their fitted parameterizations are shown in figure 8.

The performance of a particular kaon selection, using either w_i or λ_i can be evaluated by considering the efficiency for the selection and the resulting purity of a sample of kaon candidates. We define the efficiency as number of tracks which hit at least one TOF bar and pass the selection cuts divided by the total number of tracks which hit at least one TOF bar. This includes the inefficiency due to occupancy in the bars. The purity is the number of actual kaons selected in this way divided by the number of candidates selected. The gap at $z = 0$ occupied by PMT assemblies for a short bar system reduces the relative acceptance to 85% of that for a system with long bars. When studying kaon selection using a TOF system with short bars, we scale the efficiency by this relative acceptance.

6.1 Comparison of w_i- and λ_i-based selections

The weight, w_K, tests for consistency with the kaon hypothesis but does not consider other possibilities with which it could also be consistent. When the momentum of a track is above $\sim$ 1.4-1.7 GeV/c, the K-π separation power of time of flight falls below 2σ, so additional tests must be made to reject the numerous pions in this region which are also consistent kaon candidates. This can be done by either imposing a maximum momentum cut or by imposing a pion veto cut, $w_\pi < w_\pi^{\rm cut}$. The normalized likelihood is constructed to represent the probability that a particular track is a kaon given the levels of consistency with other hypotheses and their relative production fractions. Hence, no further cuts are required to purify a selection of kaons based on their normalized likelihood. Figure 9 shows comparisons of efficiency *vs* purity for various kaon selections based on particle weights or normalized

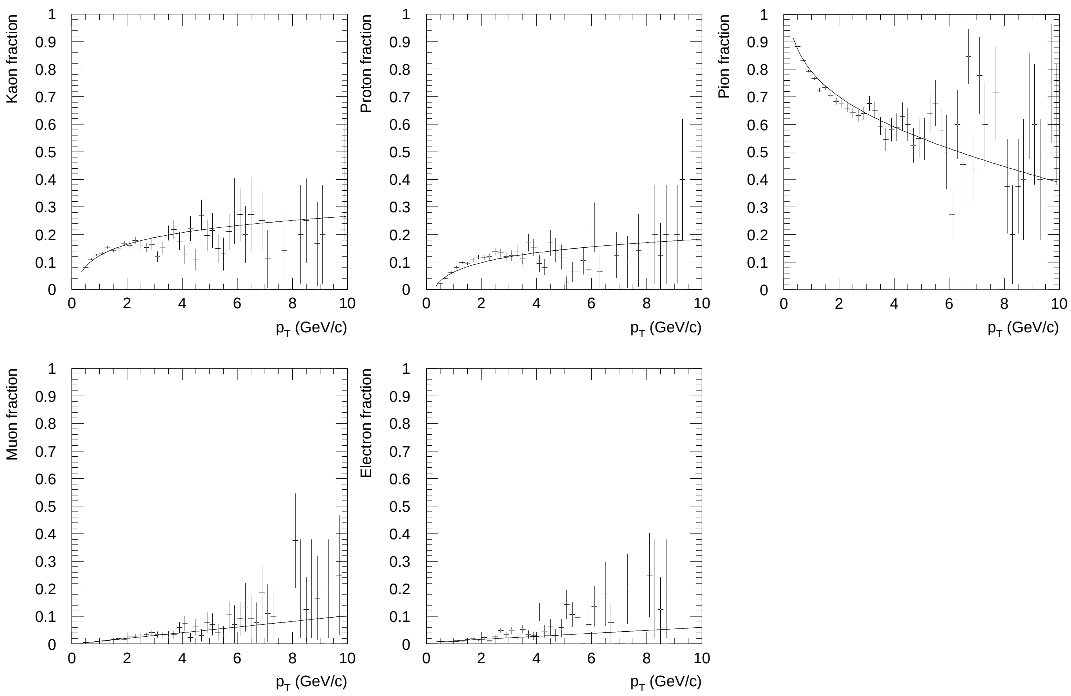

Figure 8: Particle fractions as functions of p_T. The superimposed curves are the empirical fits used to define the normalized likelihood functions. The function describing the pion fraction is constrained by $f_\pi(p_T) = 1 - f_K(p_T) - f_p(p_T) - f_\mu(p_T) - f_e(p_T)$.

likelihoods. These are

- A likelihood cut, $\lambda_K > \lambda_K^{\rm cut}$,
- A weight cut, $w_K > w_K^{\rm cut}$,
- A weight cut with an upper momentum cut, $p < 1.4$ GeV/c,
- A weight cut with a pion veto, $w_\pi < w_\pi^{\rm cut}$.

From these plots one observes that the kaon purity is generally rather low unless either a restricted momentum range or a pion veto is applied. A pion veto cut of $w_\pi < 0.05$ is seen to be generally more efficient and to have a higher purity than a momentum cut. Also, a selection based on λ_K alone is seen to provide the highest purity for a given efficiency.

6.2 Inclusion of dE/dx information

The COT will also provide some level of particle separation power *via* its measurement of the energy loss of tracks due to ionization. Although inferior to the particle identification capabilities of a TOF system at low momenta, it is natural to try to include as much of the available information as possible when forming the normalized likelihoods for a track. This is done by computing the χ^2 which compares both TOF and dE/dx measurements to their expected values for a particle of type i:

$$\chi_i^2 = \chi_i^2(TOF) + \chi_i^2(dE/dx). \tag{13}$$

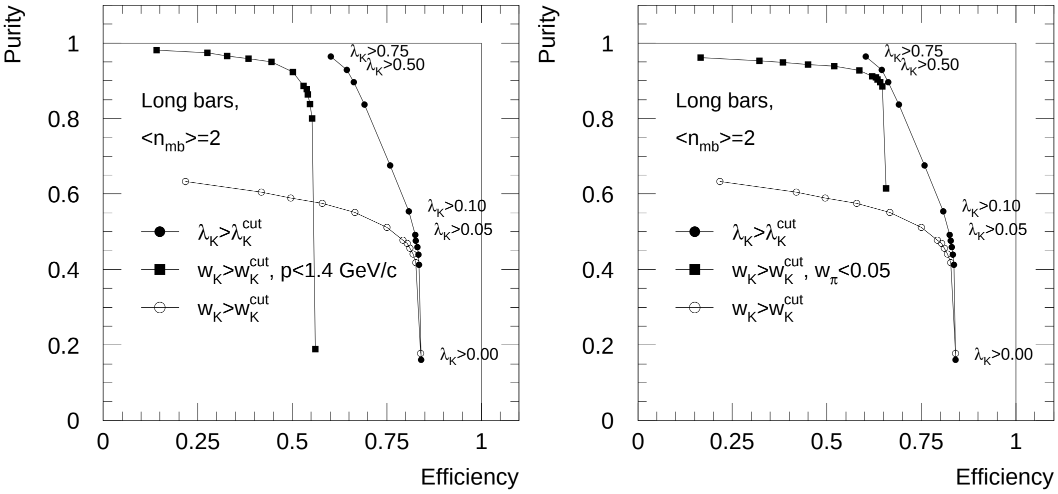

Figure 9: Comparison of efficiency *vs* purity for kaon selections based on a cut $w_K > w_K^{\rm cut}$ and various pion veto cuts and based on a normalized likelihood cut $\lambda_K > \lambda_K^{\rm cut}$. Tracks are assigned to TOF hits based on $T_L - T_R$ matching in events with $\langle n_{\rm mb}\rangle = 2$. The symbols indicate selections made at $w_K, \lambda_K > 0.00, 0.01, 0.02, 0.03, 0.04, 0.05, 0.1, 0.2, 0.3, 0.4, 0.5, 0.75$.

This is then used to compute the combined normalized likelihood variables. The improvement gained by including dE/dx information is shown in the efficiency *vs* purity plot in figure 10. This figure indicates that dE/dx provides only a minor improvement in the purity of a kaon sample of a given efficiency. Nevertheless, its inclusion does not degrade the purity, so we continue to use combined normalized likelihood variables for kaon identification. Whether or not dE/dx is used should only have a minor impact on the conclusions of any physics studies.

6.3 Comparison of track-hit association algorithms

In section 4 it was shown that the "closest track" method had a higher efficiency for associating PMT hits with tracks than did the "$T_L - T_R$" method. The comparison of the efficiency and purity of kaon tracks with PMT's associated using each algorithm is shown in figure 11. It confirms that the efficiency is always higher for the "closest track" method, as it should be, since an isolated track selected by the "$T_L - T_R$" algorithm will always be selected by the "closest track" algorithm.

There are still additional improvements in purity which can be made here. In practice, we may form a likelihood variable which measures the probability that a track is associated with a given PMT using all available information in the event. It is not clear how much of the remaining inefficiency can be recovered by techniques such as this.

6.4 Luminosity dependence of efficiency and purity

As the average number of minimum bias events increases the efficiency for associating tracks with PMT hits will be reduced. Some of this loss is reduced in a TOF system with short bars since the occupancy will be lower. However, this design has an inherent loss of acceptance

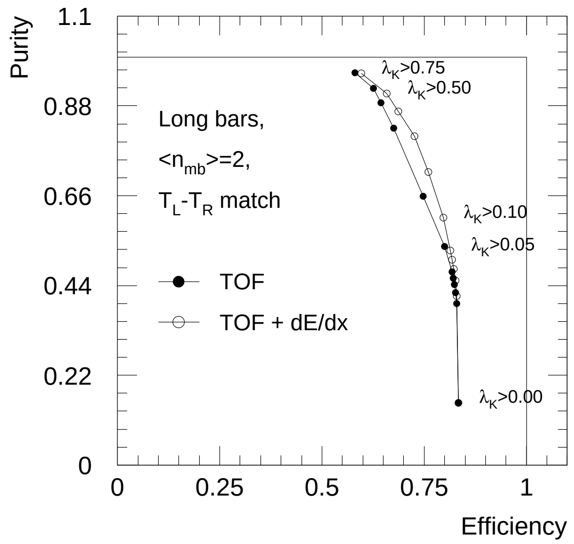

Figure 10: Efficiency *vs* purity for kaons selected using normalized likelihood variables constructed using only TOF and using a combination of TOF and dE/dx information.

due to dead space at $|z| < 20$ cm occupied by PMT's. Thus, although a system with short bars has better average timing resolution, it is not obvious that it would perform better than a system with long bars for kaon selection. Figure 12 compares the kaon efficiency *vs* purity for TOF systems with long and short bars when $\langle n_{\mathrm{mb}} \rangle = 2$ and $\langle n_{\mathrm{mb}} \rangle = 5$. The efficiency for short bars has been scaled by its relative acceptance compared with the long bar system. This indicates that the efficiency for selecting a sample of kaons with purity $> 90\%$ is larger for a TOF system with long bars except at the highest luminosities.

7 Conclusions

The level of detail incorporated into this simulation should be sufficient to obtain reliable estimates of the performance of the TOF systems studied. Below we summarize the main conclusions which can be drawn from these studies.

It was seen that we will be able to associate tracks with PMT's with high efficiency even for the highest anticipated luminosities. Although the timing resolution is degraded for tracks which are not associated with both PMT's on a bar there are still significant gains in efficiency to be made by considering this class of tracks in addition to those which have no additional hits in a bar. It is also expected that there are still minor improvements in efficiency and purity which can be made by making use of additional information which will be available in each event.

Because of the high resolution in z provided by SVX-II, additional minimum bias events will not interfere with the determination of the event t_0. A simple algorithm which refines an initial estimate of t_0, obtained using the tracks in a reconstructed B-decay, will provide measurements of the event t_0 with a resolution of about 33 ps, assuming a single PMT timing resolution of 100 ps.

The normalized likelihood variables were found to provide a convenient way to se-

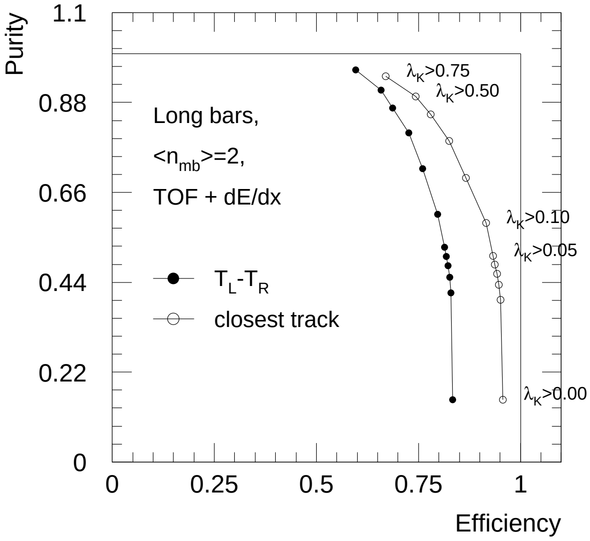

Figure 11: A comparison of the efficiency and purity for kaon samples selected using the two methods for associating PMT hits with tracks.

lect samples of kaons with optimal purity for a given efficiency. They also allow dE/dx information to be combined in a consistent way to provide a minor improvement in particle separation power. Although a TOF system with short bars was seen to suffer from a lower acceptance due to the uninstrumented region near $z = 0$, the efficiency for high purity kaon selections was seen to be very similar for both long and short TOF bars, especially for high luminosity scenarios.

Therefore we do not yet know of any fundamental limitations which would prevent us from achieving the timing precision required to have a significant impact on the Run II physics program.

8 Acknowledgments

The results presented in this note builds upon the previous work of others, in particular Bob Kephart, Joel Heinrich and Nigel Lockyer. We thank them for many useful discussions and criticisms.

References

[1] CDF Collab., *A Time-of-Flight System for CDF.* CDFNOTE 2573, Submitted to the April 1994 PAC meeting.

[2] S. Geer, *et. al.*, *A Description of the Time-of-Flight Test System.* CDFNOTE 3402, November 1, 1995.
J. Heinrich, *et. al.*, *Time-of-Flight Test System Performance.* CDFNOTE 3662, April 22, 1996.

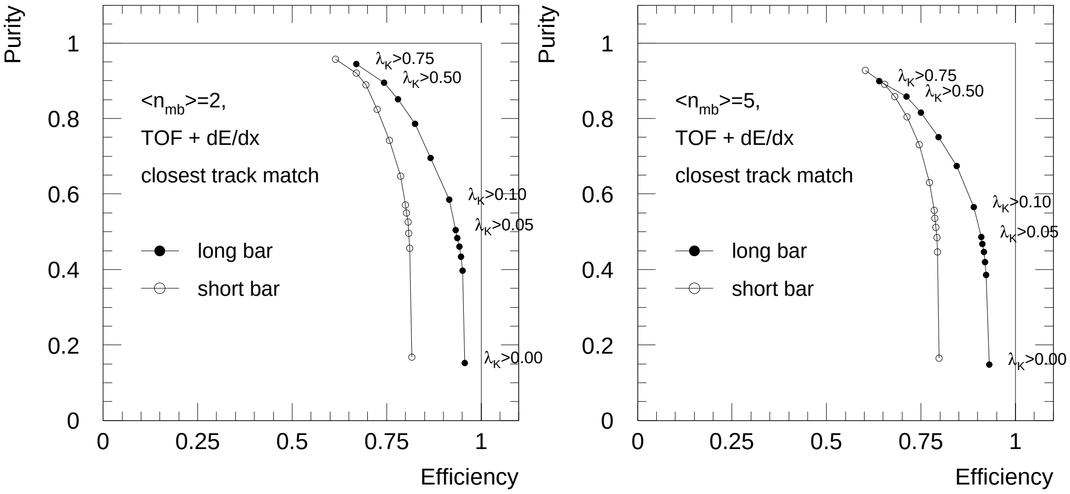

Figure 12: Comparison of kaon selection efficiency *vs* purity for long and short bar TOF systems with an average of 2 and 5 minimum bias events.

F. Ukegawa, *et. al.*, *Results from a 20-bar time-of-flight test system located inside the 1.4 T CDF solenoid.* To be submitted to NIM.

[3] M. Jones, J. Kroll and C. Chen, *B Hadron Flavor Tagging Using a Time-of-Flight Detector at CDF.* CDFNOTE 4695, August 10, 1998.

[4] F. Abe, *et al.* (CDF Collab.), K_S^0 *production in* $p\overline{p}$ *interactions at* $\sqrt{s} = 630$ *and* 1800 *GeV.* Phys. Rev. **D40** 3791-3794 (1989).

[5] Fritz DeJongh, *Proper Time Resolution for* B_s *Decays in Run II.* CDF Note 4475, March 7, 1998.